

- Press, Boca Raton, FL, ed. 74, 1994), pp. 12–50.
32. R. E. Glover, R. Baumann, S. Moser, in *Proc. 12th Int. Conf. on Low Temp. Phys.*, E. Kanda, Ed. (Keigaku, Tokyo, 1971), p. 337.
33. Within our temperature range (150 to 300 K), there were no qualitative changes in the observations.
34. In the case of Fe on Cu, the iron atoms were modeled as absorbing “black dots” to correctly model the observed interference pattern (8).
35. H. L. Davis, J. B. Hannon, K. B. Ray, E. W. Plummer, *Phys. Rev. Lett.* **68**, 2632 (1992).
36. R. Stumpf and P. J. Feibelman, *Phys. Rev. B* **51**, 13748 (1995).
37. We thank N. Ashcroft, G. Mahan, A. Overhauser, E. Tossatti, and P. Feibelman for their contributions. Supported by NSF grant DMR-9510132 (E.W.P.) and the Center for Atomic-Scale Materials Physics (sponsored by the Danish National Research Foundation, the VELUX Foundation, and the Knud Højgaard Foundation).

18 November 1996; accepted 3 February 1997

Probing the Local Effects of Magnetic Impurities on Superconductivity

Ali Yazdani,* B. A. Jones, C. P. Lutz, M. F. Crommie,†
D. M. Eigler

The local effects of isolated magnetic adatoms on the electronic properties of the surface of a superconductor were studied with a low-temperature scanning tunneling microscope. Tunneling spectra obtained near magnetic adsorbates reveal the presence of excitations within the superconductor’s energy gap that can be detected over a few atomic diameters around the impurity at the surface. These excitations are locally asymmetric with respect to tunneling of electrons and holes. A model calculation based on the Bogoliubov–de Gennes equations can be used to understand the details of the local tunneling spectra.

Superconductivity and magnetism in solids occur because of dramatically different microscopic behaviors of electrons. In a superconductor, electrons form pairs with opposing spins, whereas to produce magnetism, electrons are required to have their spins aligned to form a net local magnetic moment. The competition between these effects manifests itself in the dramatic reduction of the superconducting transition temperature when magnetic impurities are introduced in a superconductor (1). Within the context of the pioneering theoretical work of Abrikosov and Gor’kov (2) and its extensions (3, 4), a magnetic perturbation reduces the superconducting order parameter and leads to the appearance of quasi-particle excitations within the superconducting gap. Macroscopic planar tunnel junctions doped with magnetic impurities have shown sub-gap features in the superconductor’s tunneling density of states (5). No direct measurement, however, has yet been reported on the structure of a magnetically induced quasi-particle excitation on the atomic length scale around a single magnetic impurity.

We directly probed the local electronic properties of a superconductor in the vicinity of a single, isolated magnetic atom with

a scanning tunneling microscope (STM). We found that, near magnetic adatoms on the surface of a conventional superconductor, localized quasi-particle excitations at energies less than the superconductor’s energy gap are induced in the superconductor by the impurities. Previously, the STM has been used to obtain local information on the nature of the electronic excitations of a vortex in a type II superconductor (6) on length scales comparable with the superconducting coherence length ξ_0 . In contrast, the excitations reported here are detected over a few atomic diameters near the impurity, at length scales far shorter than ξ_0 . We can explain the main features of our data with a model calculation of the local electronic properties of a magnetically doped superconductor based on the Bogoliubov–de Gennes equations; however, some features of the data remain unexplained.

We performed our experiments using an ultrahigh vacuum STM, which operates at temperatures down to $T = 3.8$ K. We used a single-crystal Nb(110) sample (99.999% purity) that was cleaned by numerous cycles of ion sputtering and vacuum annealing. Niobium samples of similar quality have bulk transition temperature $T_c \sim 9.2$ K, superconducting energy gap $2\Delta \sim 3.05$ meV, and $\xi_0 \sim 400$ Å. STM images of the sample after it had been processed and cooled to low temperatures showed the sample surface to be well ordered, with terraces as large as 100 Å, and to have an acceptable terrace defect density for our

experiments. The main surface impurity was oxygen, which images as a dip in STM topographs. The local tunneling density of states (LDOS) of the Nb surface was obtained from measurement of the differential conductance dI/dV (where I is the current) of the STM junction versus sample bias voltage V (with respect to the tip) performed under open feedback loop conditions with standard low-frequency ac lock-in detection techniques. The width of the tunneling barrier (the height of the tip above the surface) during the measurements was adjusted before opening the feedback loop by setting the junction impedance R_j at an $eV \gg \Delta$. We used a polycrystalline Au wire as our tip; however, the chemical identity of the last atom on the tip is unknown.

We first measured the tunneling density of states for the Nb surface without the magnetic impurities. The spectrum in Fig. 1A is highly reproducible at different locations on the Nb surface, such as near atomic step edges and in the vicinity of surface defects such as oxygen. This spectrum can be fitted very well with the thermally broadened Bardeen-Cooper-Schrieffer (BCS) density of states (Fig. 1A) with a value of 2.96 meV for 2Δ , which is consistent with that reported for Nb, and a sample temperature of 3.85 K (7).

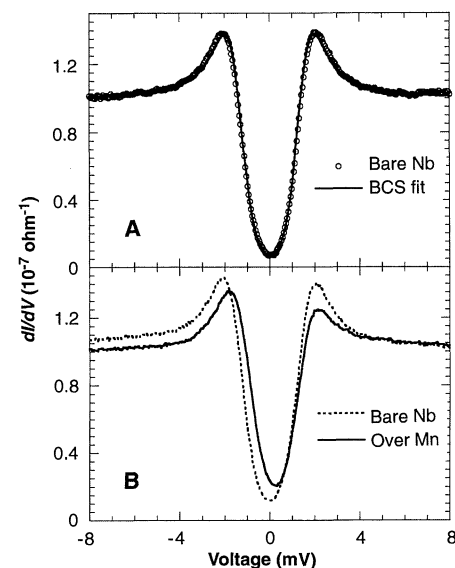


Fig. 1. (A) The dI/dV spectrum of the STM junction at $R_j = 10^7$ ohms ($V = 10$ mV) measured for the clean Nb(110) surface (open circles). The solid line is the BCS fit to the data. (B) Spectra measured ($R_j = 10^7$ ohm) near a Mn adatom. The solid line is from measurements with the tip over the adatom site and the dashed line is from measurements with the tip 16 Å away over the bare Nb surface. We used the convention that a positive bias V corresponds to electrons tunneling to the sample from the tip.

IBM Research Division, Almaden Research Center, 650 Harry Road, San Jose, Ca 95120, USA.

*To whom correspondence should be addressed. E-mail: yazdani@almaden.ibm.com

†Permanent address: Department of Physics, Boston University, Boston, MA 02215, USA.

We deposited a low coverage (about 0.005 of a monolayer) of adatoms on the cooled surface from calibrated electron-beam evaporation sources and examined the effect on the superconductor's LDOS. We chose Mn and Gd impurity atoms because of evidence for their magnetic behavior in bulk Nb (8, 9); hence they were likely candidates as magnetic impurities at the surface. As a control, we also repeated the measurements with ostensibly nonmagnetic Ag adatoms. After dosing the surface with one kind of impurity, we imaged the surface to find isolated adatoms on the terraces. The adsorbates image as bumps with heights of 1.0 Å in the case of Mn, 1.8 Å for Gd, and 0.8 Å for Ag in the STM topograph measured at $R_t = 10$ megohm.

Far away from the impurities (>30 Å), local tunneling spectroscopy showed that the LDOS is similar to that of the bare Nb surface before adatom deposition. However, in the immediate vicinity of magnetic adatoms, the LDOS was modified significantly. Spectra for Mn measured with the tip centered over an isolated Mn adatom and over

a bare Nb spot 16 Å away are shown in Fig. 1B. Near the Mn impurity, there is an enhancement of the density of the excitations at energies less than the Nb's energy gap ($|V| < 1.5$ mV) in an asymmetric fashion about the Fermi energy E_F . This asymmetric contribution within the gap is accompanied by a similarly asymmetric reduction of the state density for the states at the gap edge. As we describe below, the appearance of the low-lying bound excitations and the local asymmetry between the electron and hole excitations are distinctive signatures of the magnetism of the impurities.

The details of the impurity-induced changes of the LDOS can be seen more clearly by plotting the difference between the dI/dV spectra measured near the impurity and that measured far away from the impurity where we observed an LDOS described by BCS. Such difference spectra measured at different lateral distances relative to the center of the impurity adatom are shown in Fig. 2. The results for Mn and Gd impurities show clear peaks in the LDOS due to the bound excitations in the immediate vicinity of these impurities at energies less than the gap. The amplitude of the peaks and the sign of the asymmetry about E_F are distinct signatures of the adatom's perturbing potential, as demonstrated by the differences between the data on Mn and Gd. The Ag atoms, being nonmagnetic, appear not to modify the superconductor's LDOS near E_F in any significant way. For Mn, the largest contribution of the bound excitation to the spectra occurred when the tip was centered over the impurity site, whereas for Gd this contribution was maximum when the tip was displaced laterally by 6 Å from the center of the adatom.

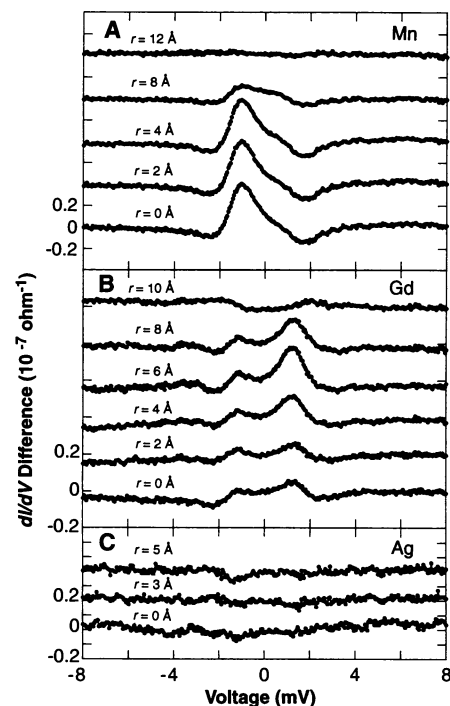
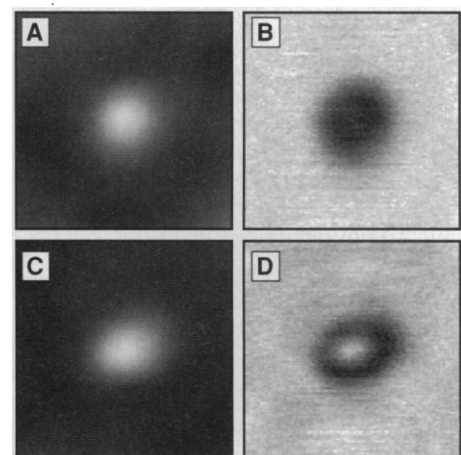


Fig. 2. The difference spectra measured near (A) Mn, (B) Gd, and (C) Ag adatoms. The presence of peaks in the data indicates the presence of excitations within the Nb's energy gap near the magnetic impurities. The data measured at different radial distances (r) are offset by a constant (4×10^{-8} ohms for Mn, 2×10^{-8} ohms for Gd, and 2×10^{-8} ohms for Ag) for clarity. The background used to obtain the difference spectra in each case was measured with the tip over the bare Nb surface about 30 Å away from the impurities.

Despite the variation, however, the impurity-induced bound excitations for both Mn and Gd impurities could only be detected within 10 Å around the impurities. These spatial characteristics are easily imaged by measuring the ac dI/dV at a fixed voltage while scanning the tip in constant dc current mode. Such images are shown in Fig. 3 along with the constant-current images for Mn and Gd adatoms. The bound-state excitation for each of the magnetic impurities is localized to the dark regions in these gray-scale images.

To account for the spectroscopic characteristics and spatial structure of the magnetic impurity-induced bound excitations observed in our experiments, we describe a model calculation of the local tunneling spectra for a classical spin impurity embedded in a bulk superconductor. In our model, we ignore the dynamics of the spin and choose a spherical geometry that ignores any possible surface effects. Self-consistent calculations by Schlottmann (10) show evidence for local suppression of the superconducting order-parameter (pair potential) on a length scale comparable with the Fermi wavelength λ_F around a magnetic impurity. However, tunneling measurements do not measure the order-parameter directly; therefore, we calculated the variation of the LDOS caused by the local changes of the order-parameter and the bound excitations predicted in (3) around the impurity. We considered the impurity to create a spin-dependent exchange potential J and an ordinary scattering potential U , which are both finite over a region of atomic dimensions with radius a around the impurity. In our model, we assumed J to be ferromagnetic; however, an antiferromag-

Fig. 3. Constant-current topographs and simultaneously acquired dI/dV images show the spatial extent of the bound state near Mn and Gd adatoms. (A) Constant-current (32 \AA by 32 \AA) topograph of a Mn adatom; $I = 1$ nA and $V = -3$ mV. Black to white corresponds to a 1.1 Å increase in the tip height. (B) Image of dI/dV near the Mn adatom, acquired simultaneously with the topograph in (A) by using an ac detection frequency above the bandwidth of the constant-current feedback loop. Black to white corresponds to a 16% increase in the signal. The areas where dI/dV is reduced (dark) show the extent of the bound state. This reversed contrast comes about because we chose a dc bias voltage well above the energy of the bound state, where the bound state affects dI/dV only indirectly by contributing to the total current I , so that the tip withdraws and reduces dI/dV . The choice of $eV \gg E_B$ (bound excitation energy) resulted in images that correspond well with the position-to-position variations seen in the dI/dV difference spectra. (C) Constant-current (32 \AA by 32 \AA) topograph of a Gd adatom; $I = 1$ nA and $V = 3$ mV. Black to white corresponds to a 2.0 Å increase in the tip height. (D) Image of dI/dV near the Gd adatom, acquired simultaneously with the topograph in (C). Black to white corresponds to an 8% increase in the signal. Similar to (B), the areas where dI/dV is reduced show the extent of the bound state. The elongated ring-shaped structure is tip-independent for atomically sharp tips.



netic interaction would produce the same results but with a change in the sign of the bound excitation's spin. In view of Schlottmann's calculations, for simplicity we assumed that the magnetic impurity suppressed the order-parameter to zero locally, for $r < a$ (where r is the radial distance from the impurity), whereas outside this region the order-parameter was taken to be constant and equal to that of pure Nb. The spatial variation of the superconductor's properties can be described with the Bogoliubov-de Gennes (BdG) equations, which are coupled Schrödinger-like equations for time-reversed pairs of states in the superconductor (11, 12). These pairs of states correspond to electron-like and hole-like states that describe, respectively, the local tunneling excitations at positive and negative sample bias. We solved the BdG equations, considering only the lowest ($l = 0$) angular momentum state to be affected by the impurity, and without requiring a self-consistency condition for the pair-potential.

Consistent with the results in (3), we found that a finite value of J breaks the time-reversal symmetry between the electron-like and the hole-like states, and the BdG equations show that there is one bound excitation with energy $E_B < \Delta$. This state, which is a mixture of both electron and hole excitations in the superconductor, contributes to the dI/dV spectra at $eV = \pm E_B$. The spatial characteristics of these contributions are governed

by the wave function of the bound excitation's electron and hole components, which oscillate with period of order λ_F , and decay with distance r from the impurity as $(1/r^2)\exp(-2r/\xi)$, where $\xi = \xi_0(\Delta/\sqrt{\Delta^2 - E_B^2})$. As shown in Fig. 4, for small r , the square of the electron and the hole components behave as $1/r^2$, and they are ultimately cut off for $r \geq \lambda_F/2$ (2.7 Å for Nb). This behavior is consistent with our observation that the bound excitation contribution to the LDOS decays rapidly within a few lattice constants near the impurity (13).

In our model, the presence of the magnetic potential that creates the bound excitation also causes a phase shift between its electron and hole components. An explicit example of this behavior is shown in Fig. 4, which displays the radial dependence of the electron and hole components for a particular value of J . A direct consequence of this phase shift is a local asymmetry in the spectra measured at positive and negative bias. The electron-hole asymmetry is largest at the impurity site and absent if the spectrum is spatially averaged over the whole system, as it is in the planar tunnel-junction experiments (5, 14). More specifically, for small $|J|$, the model shows that the bound excitation has a spin that is aligned with respect to the impurity, and the electron-like excitations are slightly favored at the impurity site. Increasing $|J|$, however, results in a monotonic increase of the phase shift (see inset of Fig. 4) and of the local asymmetry, accompanied by a shift of E_B toward the center of the gap. At a critical value of $|J| = J_c$, with $E_B = 0$ (at E_F) and the phase shift at $\pi/2$, there is a dramatic change in the nature of the bound excitation. For $|J| \geq J_c$, the bound excitation's spin becomes anti-aligned with that of the impurity, whereas at the same time the local asymmetry between the electron and the hole components switches and heavily favors the hole-like excitations (the case of Fig. 4). In this regime, a further increase in $|J|$ moves E_B

back toward the gap edge. The dramatic behavior at J_c in our model and that of Shiba's in (3) are linked with the changes in the superconductor's ground state, previously investigated by Sakurai (15), in the limit of a strong magnetic impurity. In this regime, it is energetically favorable for the superconductor to add an unpaired spin with a favorable orientation at the impurity site. Our calculations show that this change in the ground state of the superconductor is reflected in the large local asymmetry of the bound excitation probed by tunneling. The local asymmetry in our model is fundamentally caused by the potential J ; however, the spin-independent potential U can alter its strength.

Our model calculation can account for the detailed electron-hole asymmetry observed in local dI/dV measurements. This can be seen in Fig. 5, which shows a fit to the dI/dV difference spectra measured with the tip centered over the Mn adatom. To compute the fit, we calculated the wave function of not only the bound but also the extended excitations ($E > \Delta$) in the superconductor at the impurity site and have thermally broadened the results for $T = 3.8$ K. We used $J = 4$ eV and $a = 2.50$ Å (16). These parameters show that Mn adatoms act as a strong magnetic impurity on the Nb surface, a fact that seems likely considering the strong overlap of the Mn d levels with those of the Nb surface. Our model, however, does not capture the detailed spatial dependence of the spectra in the case of Gd. A more thorough theoretical treatment would require a calculation that is self-consistent and accounts for the electronic structure of the surface.

During preparation of this manuscript, we have become aware of other recent theoretical work on the local electronic properties of a superconductor with magnetic impurities relevant to our experiments (17, 18).

REFERENCES AND NOTES

1. For a review, see M. B. Maple, in *Magnetism*, H. Suhl, Ed. (Academic Press, New York, 1973), vol. V, pp. 289-325.
2. A. A. Abrikosov and L. P. Gor'kov, *Zh. Eksp. Teor. Fiz.* **39**, 1781 (1962) [*Sov. Phys. JETP* **12**, 1243 (1961)].
3. L. Yu, *Acta Phys. Sin.* **21**, 75 (1965); H. Shiba, *Prog. Theor. Phys.* **40**, 435 (1968); A. I. Rusinov, *Zh. Eksp. Teor. Fiz.* **56**, 2047 (1969) [*Sov. Phys. JETP* **29**, 1101 (1969)].
4. J. Zittartz and E. Müller-Hartmann, *Z. Phys.* **232**, 11 (1970); J. Zittartz, *ibid.* **237**, 419 (1970).
5. Initial tunneling experiments were reported by M. A. Wolf and F. Reif, *Phys. Rev.* **137**, A557 (1965). For more recent work, see W. Bauriedl, P. Ziemann, W. Buckel, *Phys. Rev. Lett.* **47**, 1163 (1981).
6. For a review, see H. Hess, in *Scanning Tunneling Microscopy*, J. A. Stroscio and W. J. Kaiser, Eds. (Academic Press, New York, 1993), pp. 427-449.
7. For this and all other tunneling spectra reported here, we examined the effect of the tip by repeating the measurements with different tips prepared from the

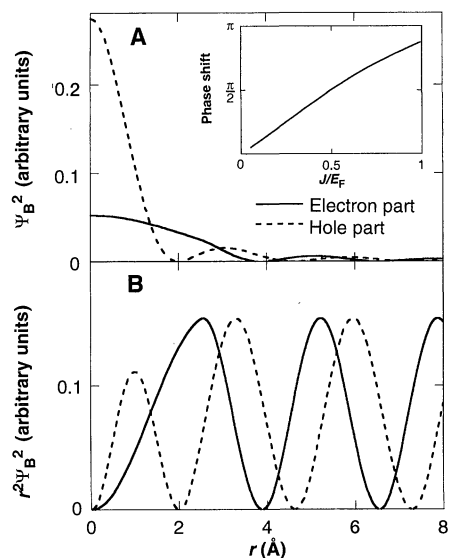


Fig. 4. The square of the electron (solid line) and the hole (dashed line) components (ψ_B) of the bound excitation's wave function created by a magnetic impurity with $J = 4$ eV and $a = 2.5$ Å. (A) The radial dependence of these functions; the inset shows the phase shift between the two components as a function of J/E_F . (B) The results in (A) are multiplied by r^2 to demonstrate the phase shift between the two components.

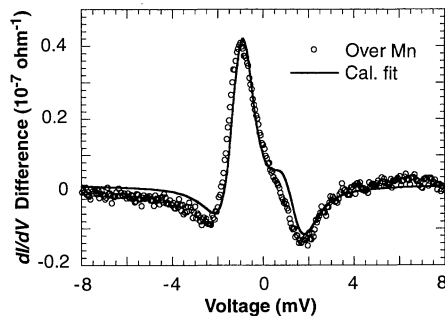


Fig. 5. Fit of the difference spectrum (open circles) measured with the tip centered over an Mn adatom by using the model calculation (solid line) of the local behavior of a superconductor near a magnetic impurity (16).

- same Au wire by (i) allowing it to collide with the Nb surface or (ii) performing field emission with it such that there was a significant change in the microscopic configuration of its outermost atoms. The results of these experiments show that the Au tips contribute little to the features in the spectra measured over the narrow range of energies near the Fermi level E_F , where we are interested in the DOS. Furthermore, our results were insensitive to the value of initial junction impedance (which determines the tip height) over 3.5 decades (10^8 to 5×10^9 ohms), except for a constant scaling factor.
8. A. Roy, D. S. Buchanan, D. J. Holmgren, D. M. Ginsberg, *Phys. Rev. B* **31**, 3003 (1985).
 9. P. D. Scholten and W. G. Moulton, *ibid.* **15**, 1318 (1977).
 10. P. Schlottmann, *ibid.* **13**, 1 (1976).
 11. P. G. de Gennes, *Superconductivity in Metals and Alloys* (Addison-Wesley, Reading, MA, 1989).
 12. Similar approaches have been used to describe STM measurements near a vortex [(6); J. D. Shore *et al.*, *Phys. Rev. Lett.* **62**, 3089 (1989); F. Gygi and M. Schluter, *Phys. Rev. B* **41**, 822 (1990)]. For more recent calculations near a vortex, see N. Hayashi, M. Ichioka, K. Machida, *Phys. Rev. Lett.* **77**, 4074 (1996).
 13. We have not made a more detailed comparison of the radial dependence between the measurement and the model calculation. Such a comparison would require us to taken into account the details of the adatom geometry, that is, the fact that at small lateral tip displacements ($r < 4 \text{ \AA}$), most of the tunneling current is channeled through the impurity site [for example, see N. D. Lang, *Phys. Rev. Lett.* **56**, 1164 (1986)].
 14. Our model predicts a local electron-hole asymmetry that oscillates and decays as a function of distance from the impurity. The $I = 0$ amplitude remains constant, but its contribution decays as a function of r . Gaussian averaging of the model calculation over typical distances averaged by STM causes a non-oscillatory but decaying asymmetry in the region near the impurity.
 15. A. Sakurai, *Prog. Theor. Phys.* **44**, 1472 (1970).
 16. Varying the parameters of the calculation, we find that for $a = 2.5 \text{ \AA}$, we can fit the data using U ranging from 0 to 0.15 E_F , while allowing J to vary by 5%. The bound excitation energy, that is, the peak location in the data, is a very sensitive function of J .
 17. M. E. Flatte and J. M. Byers, *Phys. Rev. Lett.*, in press.
 18. M. I. Salkola, A. V. Balatsky, J. R. Schrieffer, *Phys. Rev. B*, in press.
 19. We thank the authors of (17) and (18) for their interest in our experiment and thank D.-H. Lee, D. J. Scalapino, and M. Tinkham for fruitful discussions.

21 November 1996; accepted 3 February 1997

Novel Colloidal Interactions in Anisotropic Fluids

Philippe Poulin, Holger Stark,* T. C. Lubensky, D. A. Weitz

Small water droplets dispersed in a nematic liquid crystal exhibit a novel class of colloidal interactions, arising from the orientational elastic energy of the anisotropic host fluid. These interactions include a short-range repulsion and a long-range dipolar attraction, and they lead to the formation of anisotropic chainlike structures by the colloidal particles. The repulsive interaction can lead to novel mechanisms for colloid stabilization.

Dispersions of small particles in a host fluid are a widespread and important state of matter (1); colloidal suspensions are dispersions of solid particles, whereas emulsions are dispersions of liquid droplets coated with a surfactant. They are of considerable technological importance, with applications in everything from paints and coatings to foods and drugs. These are metastable rather than equilibrium systems. Attractive interactions among the particles, which arise, for example, from dispersion forces, can separate the dispersed phase from the host fluid. These forces must be counterbalanced by Coulombic, steric, or other repulsive interactions. The delicate balance between attractive and repulsive colloidal interaction determines the stability and hence usefulness of dispersions.

We report on a novel class of colloidal interactions that arise when the host fluid is anisotropic and provide a comprehensive theoretical framework to understand them.

Department of Physics and Astronomy, University of Pennsylvania, Philadelphia, PA 19104, USA.

*Present address: Institut für Theoretische und Angewandte Physik, Universität Stuttgart, Pfaffenwaldring 57, D-70550, Stuttgart, Germany.

These interactions have both repulsive and attractive components. We use general theoretical arguments and a variational procedure based on analogies with electrostatics to show how these interactions arise from the orientational elasticity of the host fluid and from topological defects therein induced by the dispersed particles. The nature of these interactions depends on boundary conditions and on the anisotropy direction of the host fluid at particle and other interfaces. Modifications in these boundary conditions can easily be produced through changes in the composition of the surfactant or host fluid, making possible a fine degree of control of colloidal interactions.

We dispersed water droplets 1 to 5 μm in diameter in a nematic liquid crystal (LC) host, pentylcyanobiphenyl (5CB), with a small amount of surfactant added to help stabilize the interface. We also used multiple emulsions, in which the nematic LC host was itself a much larger drop ($\sim 50 \mu\text{m}$ in diameter) in a continuous water phase; this isolated a controlled number of colloidal droplets in the nematic host and allowed us to readily observe their structure. The multiple emulsions were formed with

sodium dodecyl sulfate, a surfactant that is normally ineffective at stabilizing water droplets in oil. Nevertheless, the colloidal water droplets remained stable for several weeks, which suggested that the origin of this stability is the surrounding LC—a hypothesis that was confirmed by the observation that droplets became unstable and coalesced in <1 hour after the LC was heated to the isotropic phase.

We studied these nematic emulsions by observing them between crossed polarizers in a microscope. Between crossed polarizers, an isotropic fluid will appear black, whereas nematic regions will be colored. Thus, the large nematic drops in a multiple emulsion are predominately red in Fig. 1A, whereas the continuous water phase surrounding them is black. Dispersed within virtually all of the nematic drops are smaller colloidal water droplets, which also appear dark in the photo; the number of water droplets tends to increase with the size of the nematic drops. In all cases, the water droplets are constrained at or very near the center of the nematic drops. Moreover, their Brownian motion has completely ceased, an observation that is confirmed by warming the sample to change the nematic into an isotropic fluid, whereupon the Brownian motion of the colloidal droplets is clearly visible in the microscope.

Perhaps the most striking observation in Fig. 1A is the behavior of the colloidal droplets when two or more cohabit the same nematic drop: The colloidal droplets invariably form linear chains. This behavior is driven by the nematic LC—the chains break, and the colloidal droplets disperse immediately upon warming the sample to the isotropic phase. However, although the anisotropic LC must induce an attractive interaction to cause the chaining, it also induces a shorter range repulsive interaction. A section of a chain of droplets under higher magnification (Fig. 1B) shows that the droplets are prevented from approaching too closely, with the separation between droplets being a significant fraction of their diameter.

A clue to the origin of these new interactions comes from close examination of the patterns produced by the nematic host. Nematic drops containing only a single emulsion droplet invariably exhibit a distinctive four-armed star of alternating bright and dark regions that extend throughout the whole nematic drop (Fig. 1C). This pattern is produced by the rotation of the nematic anisotropy axis through a full 360° about the central water droplet and is characteristic of a topological defect called a hedgehog (2). When there is more than one water droplet, there is additional orientational texture between every pair of